Spatially resolved nuclear spin relaxation, electron spin relaxation and light absorption in swift heavy ion irradiated LiF crystals

2010 J. Phys.: Condens. Matter 22 185402

(http://iopscience.iop.org/0953-8984/22/18/185402)

J. Phys.: Condens. Matter **22** (2010) 185402 (8pp) doi:10.1088/0953-8984/22/18/185402

Spatially resolved nuclear spin relaxation, electron spin relaxation and light absorption in swift heavy ion irradiated LiF crystals

H Stork[1,2], K-P Dinse[3], M Ditter[1], F Fujara[1], W Masierak[4], R Neumann[5], B Schuster[1,5], K Schwartz[5] and C Trautmann[5]

[1] Institut für Festkörperphysik, TU Darmstadt, Hochschulstraße 6, 64289 Darmstadt, Germany
[2] Laboratoire National des Champs Magnétiques Intenses, 25 rue des Martyrs, 38042 Grenoble Cedex 9, France
[3] Fachbereich Physik, FU Berlin, Arnimallee 14, 14195 Berlin, Germany
[4] Uniwersytet Kazimierza Wielkiego, ulica Powstancow Wielkopolskich 2, 85-090 Bydgoszcz, Poland
[5] GSI Helmholtzzentrum für Schwerionenforschung, Planckstraße 1, 64291 Darmstadt, Germany

Received 22 January 2010, in final form 22 March 2010
Published 15 April 2010
Online at stacks.iop.org/JPhysCM/22/185402

Abstract
Spatially resolved ^{19}F and ^{7}Li spin–lattice relaxation rates are measured for LiF single crystals after irradiation with two kinds of swift heavy ions (^{12}C of 133 MeV and ^{208}Pb of 1.78 GeV incident energy). Like in earlier studies on ^{130}Xe and ^{238}U irradiated LiF crystals, we found a strong enhancement of the nuclear spin–lattice relaxation rate within the ion penetration depth and a slight—but still significant—enhancement beyond. By evaluating the nuclear relaxation rate enhancement within the ion range after irradiation with different projectiles, a universal relationship between the spin–lattice relaxation rate and the dose is deduced. The results of accompanying X-band electron paramagnetic resonance relaxation measurements and optical absorption spectroscopy are included in a physical interpretation of this relationship. Also the reason for the enhanced relaxation rate beyond the ion range is further discussed.

1. Introduction

This contribution is based on results reported in two recent publications describing spatially resolved nuclear magnetic resonance (NMR) experiments on LiF crystals irradiated with swift heavy ions [1, 2]. In [1], a NMR microimaging concept has been introduced and embedded into the scientific context (see references in that paper) which allows for the measurement of one-dimensional spatially resolved spin–lattice relaxation rates with a resolution of the order of 10 μm. Technical aspects of the use of large static magnetic field gradients have been discussed as well as a special data acquisition mode allowing for effectively measuring spatially resolved spin–lattice relaxation rates as low as 10^{-3} s^{-1}. The measured ^{19}F-spin–lattice relaxation rates were strongly enhanced within the ion range. But even beyond the ion range a significant enhancement was observed. The second paper [2] deals with the application of this technique to study of radiation effects by measuring spatially resolved ^{19}F- and ^{7}Li-spin–lattice relaxation rate profiles in samples irradiated with 1.44 GeV ^{130}Xe ions at fluences ranging from 10^{10} to 10^{12} ions cm^{-2}. In addition, a study of the F centre concentration n_{F} by optical absorption spectroscopy and of the concentration of paramagnetic centres n_{e} by c.w. electron paramagnetic resonance (EPR) was presented. It has been pointed out that within the ion range the fluence dependencies of the nuclear spin–lattice relaxation rate and of the EPR signal amplitude is different from that of the optically determined F centre density n_{F}, especially for high fluences.

To search for other possible ion induced defects, we recently performed ultrahigh frequency electron nuclear double resonance (ENDOR) experiments which unequivocally

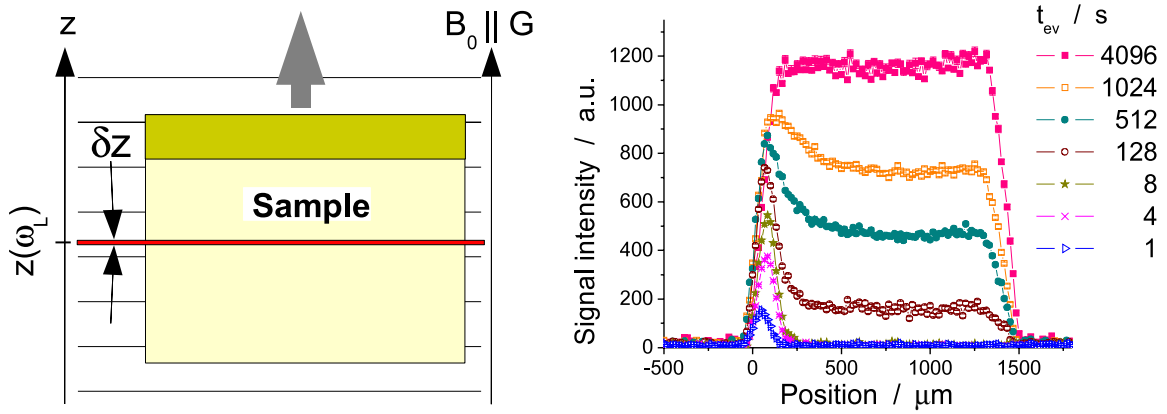

Figure 1. Left: scheme of spatially resolved NMR measurement, where the sample is moved vertically (arrow) in a huge magnetic field gradient G. The horizontal lines symbolize isolines of the magnetic field B_0. The exited slice (layer of thickness δz) remains at the position z corresponding to the central Larmor frequency $\omega_L = 2\pi\nu_L$. Right: one-dimensional ^{19}F-NMR microimages of a LiF crystal irradiated with 1.44 GeV ^{130}Xe ions of fluence 10^{11} cm^{-2} for selected evolution times t_{ev}. During t_{ev}, the nuclear spin system recovers from saturation before the signal is read out.

(This figure is in colour only in the electronic version)

confirmed the existence of F centres by identifying the hyperfine interaction parameters with the nuclear spins of several neighbour shell ions. No other types of paramagnetic centres could be observed in that study [3].

Furthermore, F centres were detected by optical means even beyond the ion range. Thus, they are most likely the direct cause for the reported [2] enhancement of the spin–lattice relaxation rate in this region.

In the present contribution the question of reconciliation of NMR relaxation rates, EPR signal intensities and optically measured F centre densities will be further dealt with. For this purpose it was important to measure the electronic spin–lattice and spin–spin relaxation times of some of the Xe irradiated LiF crystals by pulsed EPR.

In order to estimate the impact of spin diffusion on nuclear relaxation, the spin diffusion coefficient was determined from nuclear spin–spin relaxation data.

The most important aspect of this paper is a comparative study of the effects of different projectiles on nuclear spin–lattice relaxation. To this end, spatially resolved spin–lattice relaxation rates of LiF crystals irradiated with ^{12}C- and ^{208}Pb-ions were measured. Both, ^{19}F- and also some ^{7}Li spin–lattice relaxation rate profiles were recorded.

2. Experimental details

The irradiations were performed at the UNILAC linear accelerator of GSI Darmstadt. The LiF single crystals (Korth special, typical dimensions 10 × 10 × 1 mm^3) were exposed to 133 MeV ^{12}C and 1.78 GeV ^{208}Pb ions under normal beam incidence. The respective projectile range was 245 and 76 μm [4], and the applied fluences ranged from 10^8 to 10^{12} ions cm^{-2}.

The spatially resolved NMR experiments were carried out at a magnetic field of 3.8 T and a static magnetic field gradient of 74 T m^{-1}. Nuclear spins investigated were ^{19}F (ν_L = 152.3 MHz) and (to lesser extent studied) ^{7}Li (ν_L = 63 MHz). All experiments were performed at room temperature. In the case of ^{19}F-NMR, RF pulse lengths between 50 and 85 μs corresponding to thicknesses of the excited slice between 7 and 4 μm, respectively, were applied. For ^{7}Li NMR, 60–75 μs RF pulses were used, leading to a slice thickness of 14 and 11 μm, respectively. The procedure to obtain spatially resolved spin–lattice relaxation rates is illustrated in figure 1. A more detailed description of the experimental procedure can be found in [1].

Additionally to spatially resolved spin–lattice relaxation rate profiles, also a spatially resolved spin–spin relaxation rate profile was determined using a Hahn echo sequence consisting of two pulses of lengths 10 and 20 μs.

The NMR measurements were complemented by EPR and by optical absorption spectroscopy. The X-band EPR experiments were carried out on LiF samples previously irradiated with 1.44 GeV ^{130}Xe ions. Such samples have already been investigated by spatially resolved NMR and optical spectroscopy [2].

The LiF crystals were placed into thin-wall quartz tubes with an outer diameter of 5 mm. After 1 h under vacuum (at 10^{-6} mbar) the tubes were filled with helium gas and sealed. CW and pulsed EPR experiments were performed using a commercial Bruker Elexsys 680E EPR spectrometer equipped with a TerraSpec microwave bridge and a cylindrical cavity. For the temperature stabilization an Oxford helium flow cryostat was used. The temperature (10–290 K) was measured with an accuracy of 0.1 K using an Oxford ITC-503 temperature controller. The electronic spin–lattice relaxation time measurements were performed using a saturation recovery pulse sequence. The typical $\pi/2$ pulse length was 40 ns. The electronic spin phase memory times (T_{2e}) were obtained using a Hahn echo sequence ($\pi/2$–π-echo), the $\pi/2$ pulse length being 80 ns.

The optical absorption experiments were carried out at room temperature using a UV–vis spectrometer (UNICAM) in the wavelength regime of 200–800 nm. The area density of the ion induced F centres (N_F, in units of cm^{-2}) is deduced

using the Smakula–Dexter formula (oscillator strength $f_F = 0.6$ [4–6]) $N_F = 9.48 \times 10^{15} D_{opt}$, where D_{opt} is the optical density at the absorption maximum ($\lambda_{max} = 248$ nm). The accuracy of the optical density measurements is estimated to be ±2%. The F centre concentration in the irradiated samples (n_F, in units of cm^{-3}) was calculated assuming $n_F = N_F/R_I$, R_I being the ion range.

3. Results

3.1. Spatially resolved ^{19}F-spin–lattice relaxation rates

3.1.1. ^{208}Pb irradiated LiF. The spatially resolved ^{19}F-spin–lattice relaxation rate profiles of ^{208}Pb irradiated LiF crystals are plotted in figure 2 (top). As in our earlier experiments [1, 2], the following three regions can be distinguished: region (1), where the spin–lattice relaxation rate T_1^{-1} is strongly enhanced. The extension of this zone corresponds quite well to the 76 μm range of the ^{208}Pb ions [4]. There is a transition zone (2) of approximately 40 μm thickness in which the relaxation rates rapidly decrease with increasing depth. The width of this region is probably due to an artefact caused by random sample misalignment. As already discussed in [1, 2], this hypothesis is supported by the observed flank width in the signal intensity profiles, and by the fact that the magnetization recovery curves are bi-exponential.

In region 3, clearly beyond the ion range, the magnetization recovery curves are mono-exponential again. As already reported in [2] the spin–lattice relaxation rate is enhanced also beyond the ion range. The asymptotic relaxation rate deep inside the sample (region 3) slightly varies for different samples.

3.1.2. ^{12}C irradiated LiF. Figure 2 (bottom) shows spatially resolved ^{19}F-spin–lattice relaxation rate profiles of four ^{12}C irradiated LiF crystals. Due to the lower energy loss, the range of the 133 MeV ^{12}C ions is 245 μm [4] and thus much larger than for the 1.78 GeV ^{208}Pb projectiles. Note that within zone (1) the spin–lattice relaxation rate profiles for the highest fluences are quite similar to the energy loss profile calculated using the SRIM 2008 code [4] with the increased energy loss (so called Bragg peak) towards the end of the ion range.

Presumably because of stronger sample misalignment, the transition zone (2) of width up to 80 μm is more extended than for ^{208}Pb projectiles.

In zone (3), deep inside the samples, the asymptotic spin–lattice relaxation rates vary by about 50%. Since there is no clear correlation between those values and the fluences, this difference is most probably due to different concentrations of intrinsic paramagnetic impurities in the non-irradiated crystals. An increase of the relaxation rate in this zone, comparable to that reported in [1, 2], cannot be unequivocally read from figure 2 (bottom).

3.1.3. Spatially resolved ^{7}Li-spin–lattice relaxation rates. For the crystal irradiated with 133 MeV ^{12}C ions of fluence 10^{12} cm^{-2} a ^{7}Li-spin–lattice relaxation rate profile was measured (see figure 3). Both ^{19}F and ^{7}Li profiles are similar, the latter being shifted to lower rates.

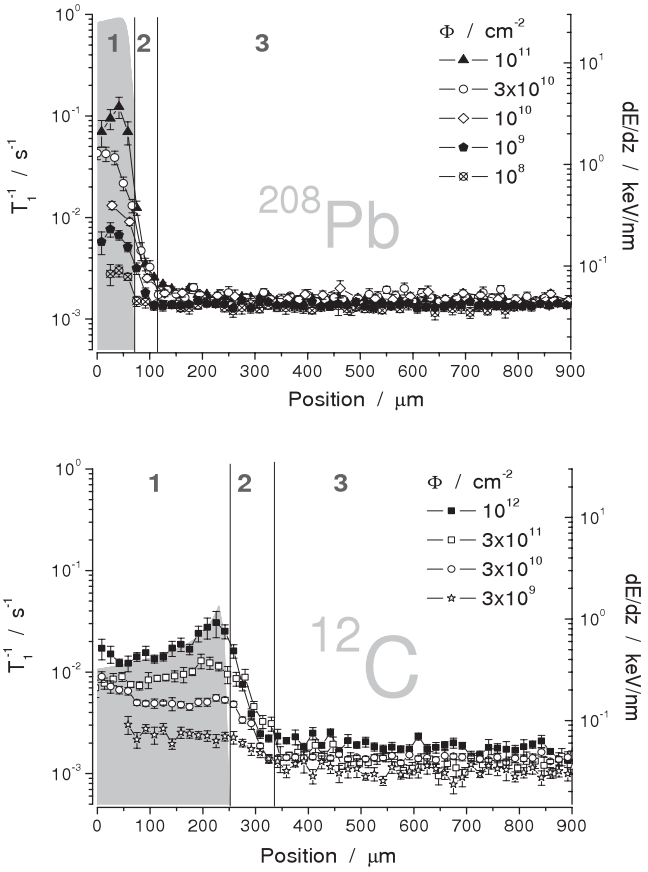

Figure 2. Position dependent ^{19}F spin–lattice relaxation rates T_1^{-1} of LiF crystals exposed to (top) 1.78 GeV ^{208}Pb ions and (bottom) 133 MeV ^{12}C ions of different fluences Φ. The filled curves denote the energy loss dE/dz (right ordinate) calculated using the SRIM code [4]. The abscissas are divided into three zones, a zone (1) within the ion range, (2) a transition zone and (3) a zone beyond the ion range.

3.1.4. Spatially resolved ^{19}F-spin–spin relaxation times. The LiF crystal irradiated with a 133 MeV ^{12}C ions of fluence 10^{12} cm^{-2} was also subjected to a measurement of the spatially resolved spin–spin relaxation time T_2 (figure 4). There is no obvious difference between the regions within and beyond the ion range. The spin–spin relaxation time averaged over all positions yields $T_2 = (53.5 \pm 1.5)$ μs.

According to [7], the spin diffusion coefficient D_s is related to T_2 by $D_s = \frac{d^2}{50T_2}$, where $d = 2.843$ Å [8] denotes the distance between ^{19}F nuclei. This yields

$$D_s = (3.02 \pm 0.09) \times 10^{-17} \text{ m}^2 \text{ s}^{-1}.$$

3.2. Electronic spin relaxation times

In order to resolve the apparent discrepancy between paramagnetic centre concentrations deduced from optical and c.w. EPR spectroscopy, some of the LiF crystals irradiated with ^{130}Xe ions were investigated by pulsed X-band EPR in order to determine the electronic spin relaxation times. Electronic spin–lattice relaxation times (T_{1e}) have been determined as well as

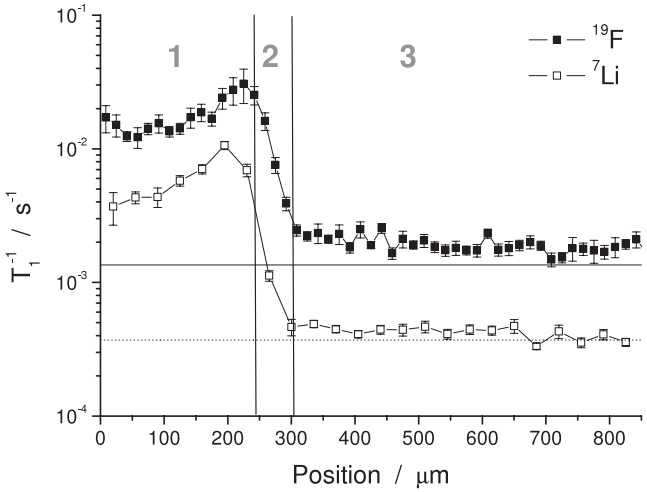

Figure 3. Position dependent ^{19}F and ^{7}Li spin–lattice relaxation rates T_1^{-1} of a LiF crystal exposed to 133 MeV ^{12}C ions of fluence 10^{12} cm^{-2}. The horizontal lines mark the ^{19}F- and ^{7}Li-spin–lattice relaxation rates of a non-irradiated LiF crystal. The abscissa is divided into three zones, a zone (1) within the ion range, (2) a transition zone and (3) a zone beyond the ion range.

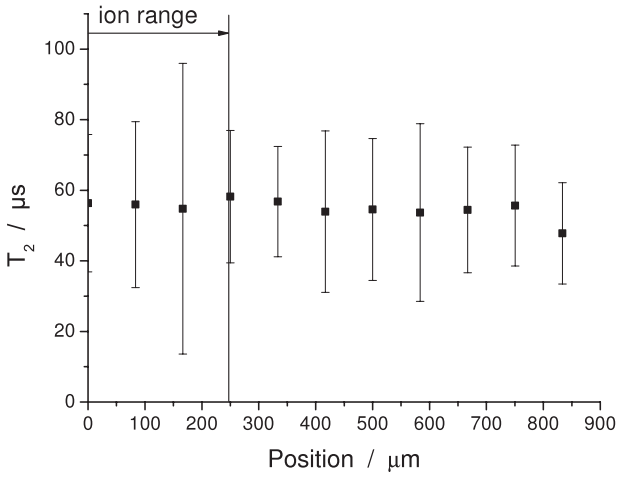

Figure 4. Position dependent ^{19}F spin–spin relaxation time T_2 of a LiF crystal exposed to 133 MeV ^{12}C ions of fluence 10^{12} cm^{-2}. The vertical line indicates the ion range.

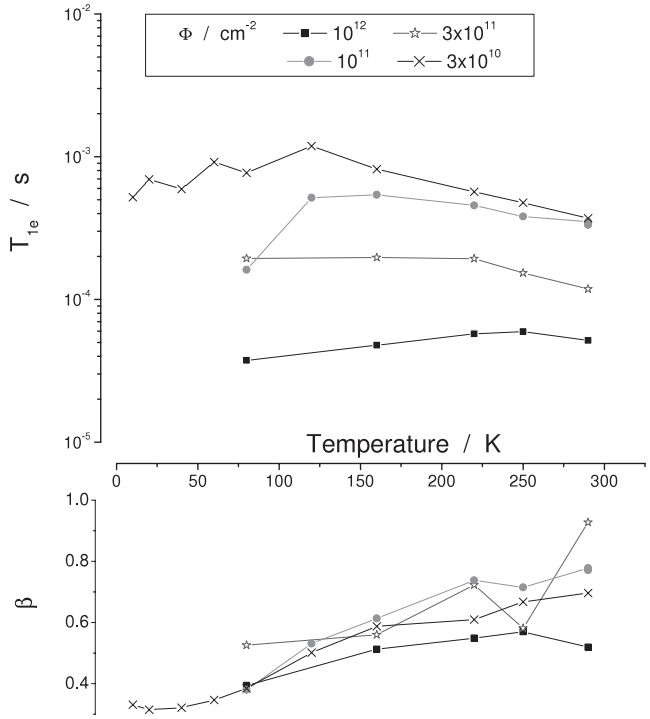

Figure 5. Electronic spin–lattice relaxation times T_{1e} and corresponding stretching exponents β of LiF crystals irradiated with 1.44 GeV ^{130}Xe ions of various fluences Φ versus temperature, determined by X-band EPR. The uncertainties are of the order of the size of the data points.

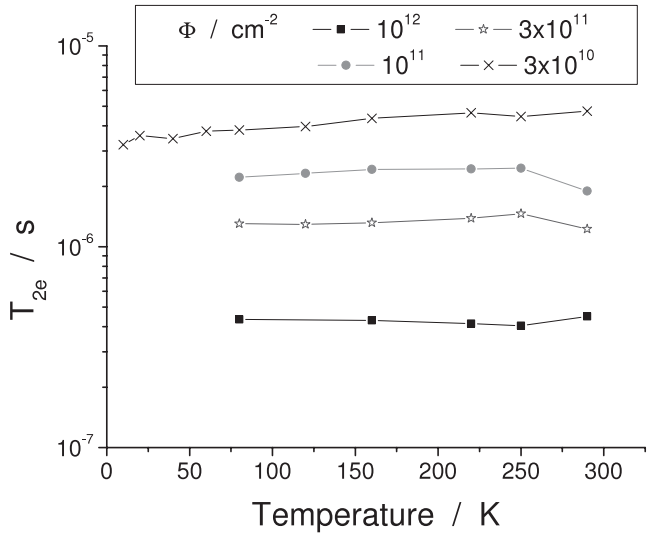

Figure 6. Electronic spin phase memory times of LiF crystals irradiated with 1.44 GeV ^{130}Xe ions of various fluences Φ versus temperature, determined by a mono-exponential fit of pulse echo decay curves. The uncertainties are of the order of the size of the data points.

electronic spin phase memory times (T_{2e}) within a temperature regime ranging from 10 to 290 K.

The T_{1e}-values were determined from fits of the observed magnetization recovery curves with a stretched exponential (Kohlrausch) function $\sim 1 - \exp[-(t/T_{1e})^{\beta}]$. Figure 5 presents the fitted T_{1e} values and stretching exponents β as a function of temperature.

According to figure 5, T_{1e} changes only slightly with temperature but decreases strongly with increasing fluence, whereas the stretching exponent β increases with temperature but shows no significant fluence dependence.

In figure 6 the electronic spin phase memory times T_{2e} are plotted versus temperature for different fluences. A decrease of T_{2e} by one order of magnitude is observed with increasing fluence, whereas no change with temperature is detected.

3.3. Optical absorption spectra

In figure 7 the optical absorption spectra of ^{208}Pb and ^{12}C irradiated LiF crystals are plotted. The absorption bands of various F_n centres are indicated [9–11]. Since only F, F_2^+,

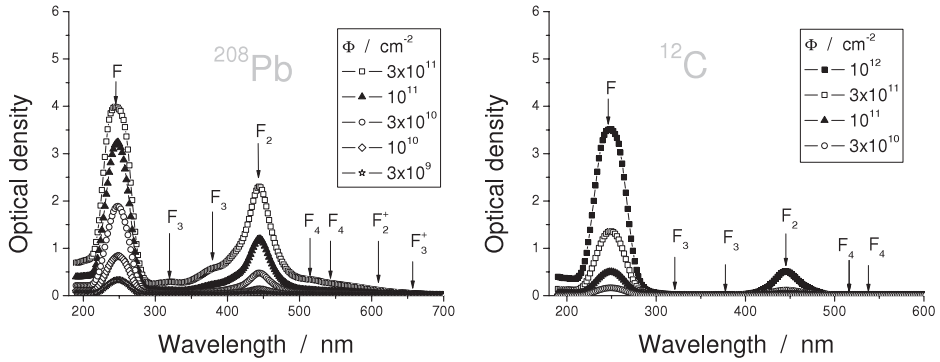

Figure 7. Optical absorption spectra of LiF crystals irradiated with (left) 1.78 GeV ^{208}Pb and (right) 133 MeV ^{12}C ions of different fluences. The expected absorption band maxima marked in the figure are taken from [9–11].

and F_3 centres are paramagnetic, all other defects should not significantly influence the spin–lattice relaxation rate. For a given fluence, the intensity of the F centre absorption bands of Pb irradiated samples is always several times higher than for crystals exposed to ^{12}C ions. This effect can also be observed for all other F_n centre absorption bands and is due to the higher energy loss of the Pb projectiles. Actually, no higher F_n centres but only F and F_2 centres can be recognized in figure 7 (right).

4. Discussion

4.1. Dose dependence of the F centre concentration and ^{19}F-spin–lattice relaxation rate

Due to the different energy loss values, the $T_1^{-1}(\Phi)$ and $n_F(\Phi)$ results of crystals exposed to different projectiles cannot be compared directly. A possible approach is to relate the data to the averaged deposited dose $D_E = \frac{\Phi E}{\rho R_I}$, where E is the projectile energy, R_I the ion range, and $\rho = 2.64$ g cm^{-3} the density of LiF. This has the advantage that observables such as n_F obtained from various ion and fluence conditions with all projectiles can be presented in a single plot. Figure 8 shows the dose dependence of the F centre concentrations n_F, determined by optical absorption spectroscopy, and the total concentration of paramagnetic centres n_e, derived previously from c.w. X-band EPR spectra (see [2]). Over a large range, both n_F and n_e are proportional to D_E, independent of the type of projectile. For a dose above about 10^6 Gy, the F centre concentration starts to saturate. This effect has been observed earlier and is described in [12]. Comparing the evolution of n_F and n_e at high doses, a different behaviour was observed, i.e., n_e continued to increase linearly with dose. Previously, this led us to the hypothesis that paramagnetic centres other than F centres might significantly contribute to n_e in this dose range [2]. However, recent pulsed ENDOR experiments on these samples gave no evidence for any significant amount of paramagnetic centres other than F centres [3]. Furthermore, using high frequency EPR it is possible to discriminate between EPR signals having a different g matrix, even if dipolar interactions might mask the g shift at the standard 9.5 GHz Larmor frequency. The gain in spectral resolution is caused by the fact that dipolar couplings are field independent, thus getting

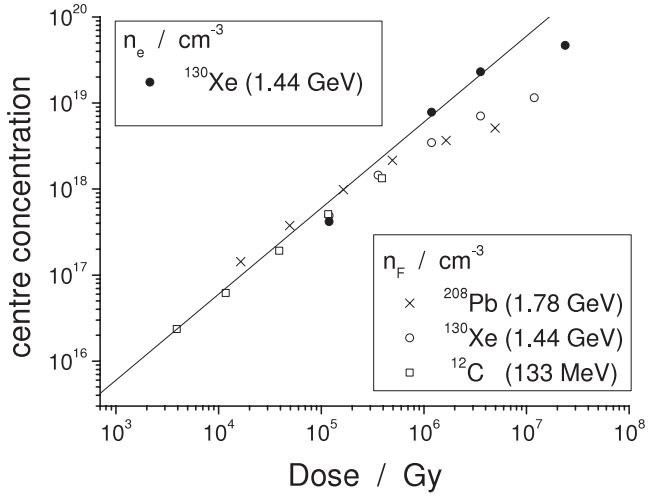

Figure 8. F centre concentration n_F determined by means of optical absorption spectroscopy and total concentration of paramagnetic defects n_e as deduced from X-band EPR assuming $M_y \sim n_e$ (compare equation (1)), i.e., neglecting saturation. The continuous line corresponds to linear dose dependence of the centre concentration. The data for ^{130}Xe ions are taken from [2].

less important at high Larmor frequencies. In our case no asymmetry of the line shape was detected at 324 GHz (see [2]), thus excluding the presence of paramagnetic centres with different g matrix signature. It therefore can be concluded that the total concentration of paramagnetic centres n_e, deduced previously from doubly integrated c.w. EPR spectra, is approximately equal to the optically determined F centre concentration n_F. Using the electronic spin relaxation data obtained by the pulsed experiments described above, we can now propose an alternative explanation for the apparent excess density n_e. Because of the rather long electronic spin–lattice relaxation times even at room temperature, the X-band EPR spectra were recorded under conditions for which saturation of the EPR transition cannot be excluded. Its impact on the evaluation of the centre concentration is briefly explained as follow: in resonance, the static solution of the Bloch equations yields the following equation for the transverse component of the magnetization, which is proportional to the signal intensity:

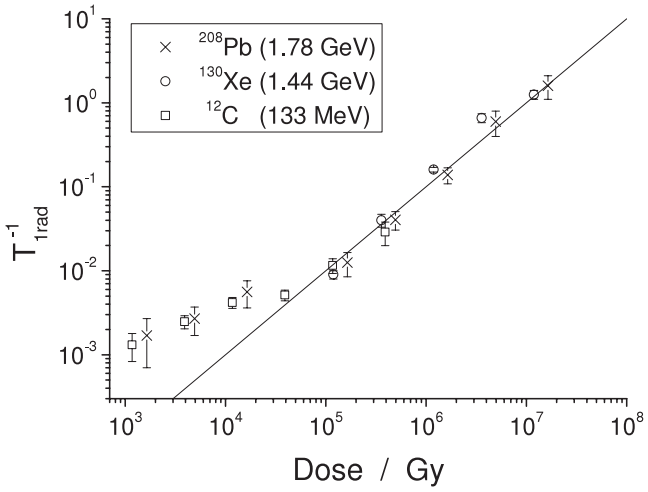

Figure 9. Dose dependence of the radiation induced peak ^{19}F-spin–lattice relaxation rates of LiF crystals irradiated with various ions. The continuous line indicates $T^{-1}_{1rad} \propto$ dose. The data for ^{130}Xe ions are taken from [2].

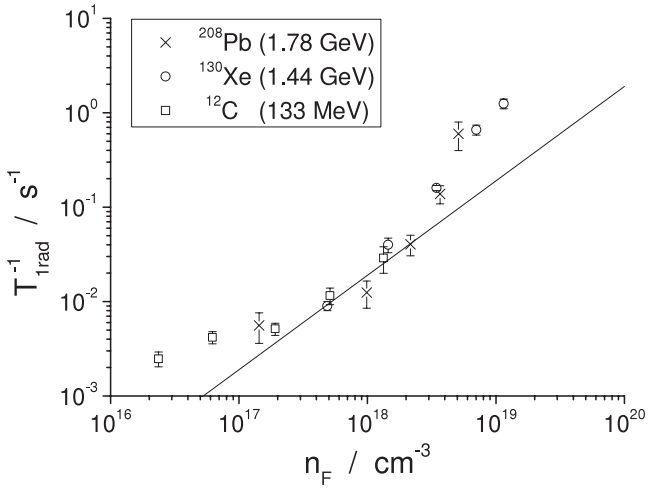

Figure 10. Radiation induced peak ^{19}F-spin–lattice relaxation rates versus F centre concentration of LiF crystals irradiated with various ions. The continuous line indicates $T^{-1}_{1rad} \propto n_F$. The data for ^{130}Xe ions are taken from [2].

$$M_y = \frac{M_0 \omega_1}{T_{2e}^{-1} + \omega_1^2 T_{1e}}, \tag{1}$$

where $M_0 \sim n_e$ is the equilibrium magnetization being proportional to the density of paramagnetic centres, ω_1 denotes the Larmor frequency corresponding to the microwave field amplitude, T_{1e} the electronic spin–lattice and T_{2e} the electronic spin phase memory time. In the case of saturation, $\omega_1^2 T_{1e} T_{2e} \gg 1$, equation (1) simplifies to $M_y \propto n_e T_{1e}^{-1}$. Applying experimental parameters used in the c.w. EPR experiment, ω_1 can be estimated to be at least 1.7×10^5 s^{-1}. With T_{1e} and T_{2e} from section 3.2, we conclude that all X-band EPR spectra have indeed been measured under conditions of saturation[6] ($\omega_1^2 T_{1e} T_{2e} \approx 1$, for $\Phi = 2 \times 10^{12}$ cm^{-2} and $\omega_1^2 T_{1e} T_{2e} > 4$, for lower fluences). In addition, we know from section 3.2 that T_{1e} depends on fluence. As long as T_{1e}^{-1} is independent of fluence (as observed for instance for a fluence of 10^{11} Xe cm^{-2}, corresponding to $D_E = 10^6$ Gy), a linear dose dependence of n_e is predicted, which should follow the optically determined n_F values. Only at elevated doses, the saturation of n_F implying a levelling off of n_e is partially compensated by the increasing T_{1e}^{-1} rate. This could explain the observed discrepancy between n_F and n_e values seen at large doses.

In figure 9, the radiation induced peak ^{19}F spin–lattice relaxation rate T^{-1}_{1rad}, i.e. T_1^{-1} corrected for the value of non-irradiated LiF, is plotted versus D_E. As found for the F centre concentration (see figure 8), the dose dependence is independent of the nature of ions used for irradiation. For $D_E > 10^5$ Gy, T^{-1}_{1rad} depends linearly on D_E. As already discussed, this is different from the dose dependence of n_F in that range. In figure 10, T^{-1}_{1rad} is directly related to n_F. For $n_F > 3 \times 10^{18}$ cm^{-3}, $T^{-1}_{1rad}(n_F)$ deviates from proportionality. This observation needs a closer analysis, in analogy to the discrepancy between n_e and n_F: under the assumption that the nuclear spin system of the samples irradiated with the highest dose is in the fast diffusion regime (which remains to be validated, see below), the paramagnetic relaxation model introduced in [13] predicts

$$T^{-1}_{1rad} \propto n_e \frac{\tau}{1 + \omega_0^2 \tau^2}, \tag{2}$$

where ω_0 is the nuclear Larmor frequency and $\tau \approx T_{1e}$. Since $\omega_0^2 \tau^2 \gg 1$, equation (2) also simplifies to $T^{-1}_{1rad} \propto n_e / T_{1e}(D_E)$. The decreasing electronic relaxation time $T_{1e}(D_E)$ in combination with a constant n_e could thus be responsible for the deviations from the proportionality $T^{-1}_{1rad} \propto n_F$ at high doses.

An estimation of the relaxation regime might be given for carbon ions at $\Phi = 10^{12}$ cm^{-2}, equivalent to $n_F \approx 1.33 \times 10^{18}$ cm^{-3}. At that concentration we find $T^{-1}_{1rad} \propto n_F$, suggesting that T_{1e} stays approximately constant implying that the relaxation model proposed in [13] is valid. In [13] three parameters are compared in order to decide in which limit the system is: first, the mean distance between F centres R_e, here 56 Å, second, a quantity B depending on the ratio of spin diffusion and dipolar coupling, here between 2.6 and 11 Å (depending on the relaxation regime), and finally a radius r_b, defining the space around a paramagnetic centre in which spin diffusions is effectively suppressed, here about 20 Å. Under these conditions we have $R_e > r_b > B$, and following [13], this suggests that the system is already close to the fast diffusion limit.

Below a F centre concentration of $n_F \approx 2 \times 10^{17}$ cm^{-3} $T^{-1}_{1rad}(n_F)$ deviates also from proportionality. The sub-linear dependence of $T^{-1}_{1rad}(n_F)$ for $n_F < 2 \times 10^{17}$ cm^{-3} is indicative of an increasing influence of each individual F centre on nuclear spin relaxation compared to higher concentrations. For ^{208}Pb irradiated LiF crystals, the transition

[6] It should be noted that in case of a strongly inhomogeneously broadened signal without structure it is in fact difficult to quantify the degree of saturation of the underlying homogeneous spin packets. In our case, because of the weak signal to noise of the very broad c. w. signal observed at 9.5 GHz, there were no hints of saturation. Just as precaution, the microwave power was reduced to 2 mW, which later turned out not to be enough, when studying the weakly irradiated samples.

occurs approximately at a fluence of 3×10^9 cm^{-2}. This corresponds to a mean distance between ion tracks of about 200 nm. At such a distance the halos containing the F centres around each ion track significantly overlap.

In the following, a tentative qualitative explanation of $T_{1\mathrm{rad}}^{-1}(n_\mathrm{F})$ in terms of F centre clustering is proposed. For isolated ion tracks, i.e., for small fluences, the F centre concentration is not homogeneous but should decrease with increasing radial distance from the ion trajectory. The relaxation behaviour of the nuclear spins thus also should strongly depend on their distance from the track centre. Within a radius of a few nanometres around the ion trajectory, the density of the paramagnetic centres is high enough such that spin diffusion is practically suppressed. There, the nuclear spins can exchange magnetization almost only directly with a paramagnetic centre. At larger distances from the track centre, spin diffusion is no longer suppressed, and the spin system is in the fast diffusion regime. At even larger distances from the track centre, the nuclear relaxation rate is finally limited by spin diffusion.

For very low fluences, equivalent to fully isolated ion tracks, one expects a linear fluence dependence of the spin–lattice relaxation rate. Due to the number of spins increasing with radial distance from the track centres, the contribution of nuclear spins in the diffusion limited regime should dominate the NMR signal. When at higher fluences the halos of several ion tracks start to overlap with each other, the F centre concentration between them increases. This leads to a gradual increase of the amount of nuclear spins in the fast diffusion regime at the expense of those in the diffusion limited regime. Due to basic considerations it is obvious that the effect of a given individual F centre on nuclear spin–lattice relaxation is stronger in the diffusion limited regime as compared to the fast diffusion regime. This directly implies a sub-linear dose dependence of the nuclear spin–lattice relaxation rate. For very high doses the ion tracks fully overlap. A further dose increase does no longer change the relaxation regime since all nuclear spins are already in the fast diffusion limit. This implies again a linear dose dependence of the nuclear spin–lattice relaxation rate. In figure 9 the crossover from the sub-linear to the linear dose dependence at a dose of about 10^5 Gy could be identified with a transition between the latter two regimes, whereas the very low dose regime is beyond the data range.

Since the relaxation model proposed in [13] assumes a uniform distribution of paramagnetic centres, it cannot explain the observed cross over from a sub-linear to a linear dose dependence.

4.2. Radiation effects beyond the ion range

As described in more detail in [1, 2] the spin–lattice relaxation rate is still enhanced beyond the ion range. This enhancement is assumed to be caused by F centres found in that range by means of optical absorption spectroscopy [2]. These centres cannot be produced by heavy ion irradiation directly, because they are located clearly beyond the ion range. They have to be created by secondary radiation originating from within the ion range. *A priori*, possible candidates for that radiation are

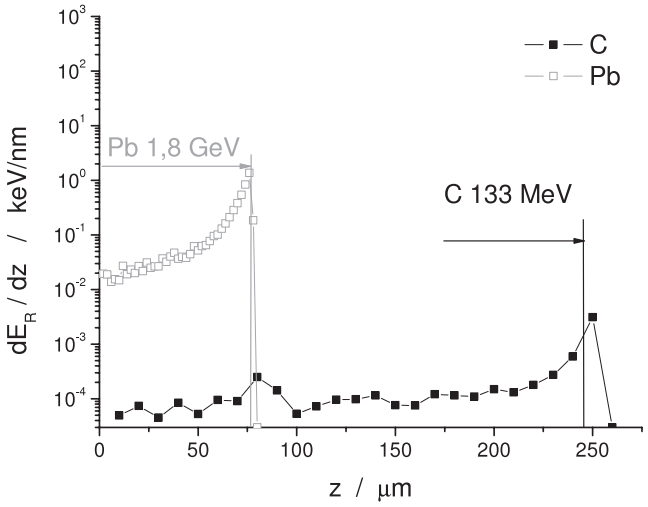

Figure 11. Electronic energy loss of recoils $\mathrm{d}E_\mathrm{R}/\mathrm{d}z$ as a function of the penetration depth z for ^{12}C and ^{208}Pb ions as calculated with the SRIM 2008 code [4]. The vertical lines mark the range of the respective primary ions.

(1) recoil atoms, (2) fragmentation of projectile nucleus and (3) x-ray emission during irradiation. Let us shortly comment on each of them.

(1) In principle recoils of energy corresponding to a range of up to several millimetres can be produced under the described circumstances—but only in the rare case of a central collision at the beginning of the ion track. In order to decide whether enough sufficiently energetic recoil atoms are produced to explain the observed enhancement of the spin–lattice relaxation rate beyond the ion range, their electronic energy loss $\mathrm{d}E_\mathrm{R}/\mathrm{d}z$ has been calculated using the SRIM 2008 code [4] (see figure 11). The recoils are obviously stopped at a depth slightly beyond the range of the primary ions. This suggests that recoil atoms cannot enhance the spin–lattice relaxation rate in a distance of even more than hundred micrometres beyond the ion range, as observed in [1, 2].

(2) According to the paper of Czudek *et al* [14], fragmented projectiles could indeed be candidates for defect creation beyond the range of the initial ^{12}C ions. However, at present we have to defer this discussion because for ^{12}C projectiles the relaxation enhancement beyond the ion range turned out not to be significant enough (see figure 3). In contrast, fragmentation for ^{130}Xe and heavier projectiles can be excluded since the closest distance between projectiles and target nuclei is always larger than the effective range of the nuclear forces.

(3) Energetic ions travelling through solids are known to emit x-rays (see [15, 16] and references within). In an independent experiment, the x-ray emission of LiF crystals under irradiation with 1.43 GeV ^{129}Xe and 2.64 GeV ^{238}U projectiles was studied at the UNILAC linear accelerator of GSI Darmstadt. The x-rays were recorded using a CdTe detector. No bremsstrahlung from δ-electrons but strong characteristic x-ray emission was observed in the energy range of 9–40 keV for ^{129}Xe ions and 15–25 keV for ^{238}U ions (a more detailed description will be published elsewhere). Such high energy x-rays can induce colour centres in LiF crystals

far beyond the ion range. Note that, different from ^{129}Xe and ^{238}U, characteristic x-rays form ^{12}C projectiles cannot produce F centres significantly beyond the ion range since their energy of about 300 eV, corresponding to a range of less than 1 μm, is far too low.

4.3. Comparison of ^{7}Li- and ^{19}F-spin–lattice relaxation rate profiles

As described in [2], the ^{7}Li-relaxation rates were found to be about an order of magnitude smaller than the ^{19}F-relaxation rates within the ion range and a factor of 3–4 in the remaining of the crystal. In this work we observe a factor of 3–4 not only beyond but also within the ion range of carbon ions. We tentatively ascribe this result to the light projectiles and correspondingly low energy loss but at present the limited available data set does not allow for a quantitative discussion of this phenomenon.

5. Conclusions

The dose dependence of the spin–lattice relaxation rates within the ion range of samples exposed to ^{12}C, ^{130}Xe and ^{208}Pb projectiles is independent of the nature of ions used for irradiation. Only in a medium dose range, a linear relationship between the spin–lattice relaxation rate and the F centre concentration exists. The deviation from established relaxation theory at low doses is assigned to a cluster effect. At very high doses, the deviation from the proportionality is caused by a change of the electronic spin relaxation times leading to a stronger effect of the F centres on the nuclear spin–lattice relaxation rate. The apparent discrepancy between the concentration of paramagnetic defects determined by c.w. EPR and optical spectroscopy, which had been reported in [2], can be resolved by considering the dose dependence of the electronic relaxation times. The enhancement of the spin–lattice relaxation rate beyond the ion range is probably caused by the emission of characteristic x-rays. A comparison of the ^{7}Li- and the ^{19}F-spin–lattice relaxation rates indicates a qualitatively different behaviour of samples irradiated with ^{12}C ions from those irradiated with heavier ^{130}Xe ions.

6. Outlook

We are working on an improved NMR spectrometer to be used for spatially resolved spin–lattice relaxation rate measurements. Apart from a better alignment of the sample the new setup will allow for spatially resolved temperature and field dependent relaxation rate measurements. Thereby, field dependent measurements of spin–lattice relaxation will possibly give further confirmation of the physical origin of the enhanced relaxation rate beyond the ion range.

Also annealing experiments can now be conducted providing information about the distribution of different paramagnetic defect types along the ion tracks.

References

[1] Stork H, Hamburger A, Gädke A, Fujara F and Schwartz K 2008 *J. Phys.: Condens. Matter* **20** 275236
[2] Stork H, Dinse K-P, Fujara F, Hamburger A, Jakes P, Neumann R, Schwartz K and Trautmann C 2008 *J. Phys.: Condens. Matter* **20** 465215
[3] van Tol J, Dinse K-P, Stork H, Schuster B, Schwartz K and Fujara F, in preparation
[4] Ziegler J F, Ziegler M D and Biersack J P 2006 http://www.srim.org/
[5] Perez A, Balanzat E and Dural J 1990 *Phys. Rev.* B **41** 3943
[6] Schwartz K, Trautmann C, El-Said A S, Neumann R, Toulemonde M and Knolle W 2004 *Phys. Rev.* B **70** 184104
[7] Rorschach H E 1964 *Physica* **30** 38
[8] http://www.korth.de
[9] Perez A, Davenas J and Dupuy C H S 1976 *Nucl. Instrum. Methods* **132** 219
[10] Hughes A E and Jain S C 1979 *Adv. Phys.* **28** 717
[11] Thévenard P, Guiraud G, Dupuy C H S and Delaunay B 1977 *Radiat. Eff.* **32** 83
[12] Schwartz K, Trautmann C, Steckenreiter T, Geiß O and Krämer M 1998 *Phys. Rev.* B **58** 11232
[13] Lowe I J and Tse D 1968 *Phys. Rev.* **166** 279
[14] Czudek J, Jarczyk L, Kamys B, Magiera A, Siudak R, Strzałtowski A, Styczeń B, Hebenstreit J, Oelert W, von Rossen P, Seyfarth H, Budzanowski A and Szczurek A 1991 *Phys. Rev.* C **43** 1248
[15] Horvat V, Watson R L and Blackadar J M 1998 *Phys. Rev.* A **57** 3635
[16] Golden J and McGuire J H 1974 *Phys. Rev. Lett.* **32** 1218